

Evanescent-Wave Cavity Ring-Down Spectroscopy for Enhanced Detection of Surface Binding Under Flow Injection Analysis Conditions

L. VAN DER SNEPPEN, J. B. BUIJS, C. GOOIJER, W. UBACHS, and F. ARIESE*

Laser Centre, Vrije Universiteit, De Boelelaan 1081–1083, 1081 HV Amsterdam, The Netherlands

The feasibility of liquid-phase evanescent-wave cavity ring-down spectroscopy (EW-CRDS) for surface-binding studies under flow-injection analysis (FIA) conditions is demonstrated. The EW-CRDS setup consists of an anti-reflection coated Dove prism inside a linear cavity (with standard or super-polishing of the total internal reflective (TIR) surface). A teflon spacer with an elliptical hole clamped on this surface acts as a 20 μL sized flow cell. The baseline noise of this system is of the order of 10^{-4} absorbance units; the baseline remains stable over a prolonged time and the prism surface does not become contaminated during repeated injections of the reversibly adsorbing test dyes Crystal Violet (CV) and Direct Red 10 (DR10). At typical FIA or liquid chromatography (LC) flow rates, the system has sufficient specificity to discriminate between species with different surface affinities. For CV a much stronger decrease in ring-down time is observed than calculated based on its bulk concentration and the effective depth probed by the evanescent wave, indicating binding of this positively charged dye to the negatively charged prism surface. The amount of adsorption can be influenced by adjusting the flow rate or the eluent composition. At a flow rate of 0.5 mL/min, an enrichment factor of 60 was calculated for CV; for the poorly adsorbing dye DR10 it is 5. Super-polishing of the already polished TIR surface works counter-productively. The adsorbing dye Crystal Violet has a detection limit of 3 μM for the standard polished surface; less binding occurs on the super-polished surface and the detection limit is 5 μM . Possible applications of EW-CRDS for studying surface binding or the development of bio-assays are discussed.

Index Headings: Evanescent-wave cavity ring-down spectroscopy; EW-CRDS; Flow injection analysis; FIA; Surface interactions; Silica surface; Crystal violet.

INTRODUCTION

Cavity ring-down spectroscopy (CRDS) is an absorbance spectroscopic technique that is based on the measurement of the decay rate of light after abrupt termination of the excitation of a high-finesse optical resonator. It has certain advantages over conventional absorbance spectroscopy: since it is a multi-pass technique, extremely low concentration detection limits are feasible. Alternatively, analytes with low extinction coefficients or in very thin layers can still be detected. Furthermore, since it is based on the measurement of the rate of decay of light rather than the measurement of $\Delta I/I_0$, sources with high intensity fluctuations such as pulsed lasers can be used. CRDS is well established and widespread in the gas phase, and applications of CRDS to liquid-phase studies are currently being developed.^{1,2}

A special mode of CRDS that is gaining considerable interest is evanescent-wave cavity ring-down spectroscopy (EW-CRDS), a technique that combines the high sensitivity of the CRDS technique with surface-specificity. In EW-CRDS,

one or more of the reflections inside the optical resonator are a total internal reflection (TIR) event. Only light of the evanescent wave associated with this TIR event is used for probing the sample. The evanescent wave decays exponentially with distance from the surface, and hence mostly species that are near, physisorbed, or chemisorbed to the surface will interact with the radiation field. The penetration depth of the evanescent wave is typically on the order of one wavelength or less. This explains the current interest in evanescent-wave-based techniques for detecting surface binding phenomena including bio-assays on surfaces.^{3–5}

Currently, three different implementations of EW-CRDS have been explored. The use of a monolithic ring cavity was already suggested and demonstrated a decade ago^{6,7} by Pipino et al. In follow-up studies, monolithic or folded resonators were used;^{8–10} this is an elegant solution to minimize intrinsic cavity losses, but the requirements on the surface quality, the morphology of the TIR surfaces, and the purity of the resonator material are very stringent. The principle of fiber-loop CRDS has been explored by O'Keefe's group, who constructed a high-finesse fiber cavity by utilizing fiber-Bragg gratings (FBGs) as reflectors.¹¹ Independently, this technique was developed in the groups of Loock and Lehmann by looping the fiber onto itself and using input and output couplers for the injection and detection of the pulse train.^{12,13}

The use of intra-cavity elements is the most straight-forward method to create an EW-CRDS setup:^{14–21} off-the-shelf or easy-to-produce custom-made optics can be used. Obviously, the surfaces placed inside the cavity cause reflection and refraction losses that affect the performance of EW-CRDS and the achievable detection limits. Possible intra-cavity elements include Dove prisms placed inside a linear cavity, standard right-angle prisms, and Pellin–Broca prisms. However, to ensure TIR at a silica–liquid interface, the angle of incidence on the TIR surface should be larger than about 66° ; hence, a linear cavity with a right-angle or Pellin–Broca prism is not appropriate for liquid-phase EW-CRDS studies on glass or quartz TIR surfaces. Usually, an anti-reflection coating is applied to minimize reflection losses at the entrance and exit surfaces.

Normal-incidence geometries have several advantages over non-normal incidence geometries. Firstly, when (relatively) small cavities are used, additional reflection losses of the surfaces can be maintained within the cavity.²² In addition, both *s*- and *p*-polarized light can be used, permitting orientational studies using the dichroic ratio. The use of a triangular prism in a ring cavity was explored by the group of Zare, to determine the molecular orientation of a film of methylene blue at the air–silica interface.¹⁷

Shaw et al. studied adsorption isotherms of Crystal Violet to silica as a function of pH and in the presence of other

Received 25 July 2007; accepted 7 March 2008.

* Author to whom correspondence should be sent. E-mail: ariese@few.vu.nl.

cations^{14,15} using an anti-reflection coated ($R \leq 0.25\%$) Dove prism inside a cavity. Furthermore, the adsorption isotherm of hemoglobin from urine samples was determined in order to assess the feasibility of using EW-CRDS diagnosis in hemoglobinuria.¹⁶ Adsorption of a charged and an uncharged dye at the silica/CH₃CN surface has been measured by Fan et al.¹⁹ using a similar setup. Mazurenka et al. built an electrochemical cell on top of an anti-reflection coated, standard right-angle prism inside a ring cavity.²⁰ Simultaneous EW-CRDS and cyclovoltammetry measurements allowed the determination of concentration changes of chromophoric [Fe(CN)₆]³⁻ upon oxidation of [Fe(CN)₆]⁴⁻. Everest et al. used a custom-made Dove prism with entrance and exit faces at normal incidence.²¹ The adsorption isotherm of hemoglobin to the silica interface as well as the average orientation of the hemoglobin transition dipole moment was measured.

Until now, liquid-phase EW-CRDS studies have included steady-state measurements^{16,21} or measurements with an extremely low continuous flow (on the order of mL/h) of sample in a 190 μ L sized flow cell.^{14,15} The experimental conditions were such that adsorption equilibrium could be reached and thermodynamic properties could be measured; reversibility was not a critical factor. In contrast, our ultimate goal is the immobilization of biomolecules such as monoclonal antibodies and to detect compounds of interest showing interaction with these biomolecules using flow injection analysis (FIA) or liquid chromatography (LC). The use of biologically modified surfaces will be the subject of forthcoming studies. In this paper the test compounds Crystal Violet (CV) and Direct Red 10 (DR10) on unmodified surfaces are used to examine the performance of EW-CRDS detection under flow injection analysis (FIA) or liquid chromatography (LC) conditions. A generally encountered difficulty when using such test compounds is their irreversible adsorption to the TIR surface, necessitating rigorous cleaning (applying acids or alkaline solutions) or even etching of the surface after each measurement. An important next step in liquid-phase EW-CRDS is making such measurements compatible with FIA or LC by minimizing the flow cell dimensions, using flow rates on the order of mL/min, and having control over the adsorption process so that the TIR surface can be used over a prolonged time for repeated measurements.

In this study, flow injection measurements of the positively charged dye CV and the negatively charged dye DR10 are compared. The addition of an organic modifier to the eluent—as is quite common in reversed-phase LC—ensures a reversible chromatography-like adsorption process. The observed ring-down times are converted to absorbance units and compared with the predicted values in the absence of adsorption based on the layer thickness probed by the evanescent wave; the difference indicates specific surface binding. The hydrophilic, negatively charged silica surface shows a strong preference for CV over DR10. The adsorption of CV could be dramatically increased by lowering the flow rate; for DR10 such effects are far less pronounced. It should be stressed that the scope of the present study is to explore conditions for the application of EW-CRDS in flow systems or LC rather than the characterization of the test molecules used. Since the adsorption properties of CV have been investigated previously in several studies,^{14,15} CV was chosen for testing the reversibility of adsorption to the surface.

EXPERIMENTAL

Crystal Violet (CV, color index 42555, 98%, $\epsilon_{532} = 5.3 \times 10^4 \text{ M}^{-1}\text{cm}^{-1}$) was obtained from Aldrich Chem. (Milwaukee, WI) and Direct Red 10 (DR10, $\epsilon_{532} = 1.0 \times 10^4 \text{ M}^{-1}\text{cm}^{-1}$) was obtained from Sigma-Aldrich (Seelze, Germany). Solutions of CV, diluted from a 0.2 mM stock solution in Milli-Q and DR10 were prepared in the eluent that was used. The eluent was 50% (v/v) 10 mM potassium phosphate buffer (pH = 4.3, 7.4, or 8.8) in HPLC-grade methanol; a flow of 0.5, 0.3, or 0.1 mL/min was delivered using an LC-pump; and 100 μ L of sample was injected using a six-way injection port. The eluents were degassed by sonication before use. In order to test the influence of the buffer and the ionic strength on adsorption of CV to the surface, 10 mM HEPES (4-(2-hydroxyethyl)piperazine-1-ethanesulfonic acid) buffer at pH 7.4, as well as 100 mM phosphate and HEPES buffers, were used in the eluent with 50% of methanol as well. A cell with a volume of 20 μ L was constructed by clamping a 1 mm thick teflon spacer with an elliptical hole of 9.4×3.5 mm on top of a Dove prism (see Fig. 1). Two anti-reflection coated ($R \leq 0.25\%$ at 532 nm, $n = 1.52$, 45° facets) BK7 Dove prisms (Casix, Fuzhou, China) were used, one with a surface roughness rms ≤ 1.5 nm, $\lambda/2$ at 632.8 nm as received from the manufacturer (“standard polish”) and one with a custom polishing (Layertec, Germany, surface roughness rms ≤ 0.2 nm, $\lambda/10$ at 632.8 nm). Cleaning was performed by simply wiping the TIR surface of the prism with water or methanol.

A cavity was constructed using mirrors ($R \geq 99.996\%$ at 532 nm, 50 mm radius of curvature) from REO Inc. (Boulder, CO). Alignment of the Dove prism inside the linear cavity was relatively easy: the laser was centered on the entrance and exit mirror holders, using two pinholes, and was then optimized with the mirrors in place. In the absence of the Dove prism, this yielded a ring-down time of several microseconds. Next, the mirrors were replaced with the pinholes again, and the Dove prism (which was already in place on the prism mount) was inserted by vertical movement of the prism mount using a micrometer screw. A combination of horizontal and angle movement of the prism was used to make sure that the beam path is not altered by the Dove prism. The prism mount was subsequently moved out of the beam path and the mirrors were inserted and aligned again by optimizing the ring-down transient behind the linear cavity. The Dove prism was inserted again, and the photomultiplier tube (PMT) was moved under an angle of 90 degrees of the cavity axis so that the scatter losses of the exit face of the Dove prism ($R \leq 0.25\%$ on each pass) are detected.²⁰ This ensures that more light (0.25% on each pass, rather than 0.004%) will reach the detector. Ring-down times for both the super-polished and standard polished TIR surfaces were between 20 and 25 ns, indicating that the surface roughness of the TIR surface of the prisms does not contribute significantly to the total losses of the system. This short ring-down time is on the order of the maximum achievable ring-down time with the current cavity: with the anti-reflection coatings specified at $R \leq 0.25\%$ per surface and with two surfaces per pass, 200 passes are expected. Considering the relatively short cavity (85 mm), this corresponds to a ring-down time of 57 ns. Of course, additional reflection and scatter losses will take place, resulting in a ring-down time on the order of 20 to 25 ns. The fact that about 10% of the original ring-down time of the empty cavity is maintained after

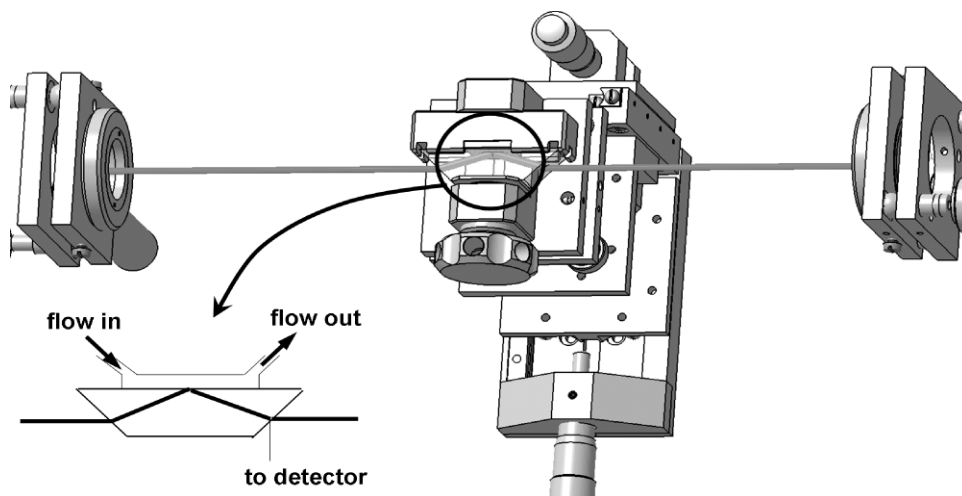


FIG. 1. Schematic of the EW-CRDS setup (not drawn to scale). An anti-reflection-coated Dove prism is mounted on a mirror holder in a 70 mm long linear cavity. The effective path length with the prism in place, taking into account the refractive index, is 85 mm. Reflection loss at the 45° exit surface is used for detection of the transient. A teflon spacer with an elliptical hole is clamped leak-tight on the TIR face of the prism, and flow is delivered by PEEK tubing connected with finger-tights. The mirror holder, mounted on an x,z-stage permitting horizontal and vertical movement, enables two degrees of freedom for tilting and in-plane rotation.

insertion of an intra-cavity element is quite common (for example, Ref. 14).

Laser pulses at a wavelength of 532 nm, 2.4 ns duration, and a nominal bandwidth of $\approx 10 \text{ cm}^{-1}$ were used to excite the cavity. As previously discussed, excitation with narrow-band radiation from injection-seeded Nd:YAG lasers would result in mode-beating on the transients,²³ and therefore the 532 nm radiation at sufficiently large bandwidth was produced through the use of an optical parametric oscillator (OPO) pumped with the third harmonic of a Coherent Infinity single-mode Nd:YAG laser (Santa Clara, CA) at 355 nm;² this laser has the advantage that the repetition frequency can be varied between 10 and 100 Hz without modifications to the beam profile.

For the CRDS measurements no mode-matching was performed, ensuring multi-mode excitation of the cavity. The optical path length was $L = 85 \text{ mm}$ (including a correction for the Dove prism with $n = 1.52$). A scheme of the setup is shown in Fig. 1; the laser beam was p -polarized with respect to the 45° facets of the prism. Transients were recorded using a photomultiplier tube (Hamamatsu, Shimokanzo, Japan) and a fast sampling oscilloscope of 1 GHz analog bandwidth (Tektronix 5104 5 GS/s). An auxiliary photodiode was used to trigger the detection system. Typically, the first 15 ns of the detected trace, which contains the instrumental response function, was rejected; 65 ns (corresponding to about three ring-down times τ_0) of the remaining trace was fitted. A moving average of 1 second or 100 data points was applied afterwards. Absorbance units (ϵCl) were derived from the ring-down times via the following equation:

$$\epsilon Cl = \frac{\alpha_{\text{anal}} l}{2.303} = \frac{L}{2.303c} \left(\frac{1}{\tau} - \frac{1}{\tau_0} \right) \quad (1)$$

where ϵ is the molar extinction coefficient in $\text{M}^{-1}\text{cm}^{-1}$ at 532 nm, C is the concentration in M, and l is the effective path length of the evanescent wave through the sample in cm. L is the cavity length ($85 \times 10^{-3} \text{ m}$), c is the speed of light, α_{anal} is the absorption coefficient in cm^{-1} , τ and τ_0 are the ring-down times in the presence or absence of analyte. In the case of

adsorption to the surface, the local concentration C will increase, leading to a shorter ring-down time τ .

RESULTS AND DISCUSSION

In view of our future applications, the performance of EW-CRDS is examined at flow rates that are compatible with FIA and LC (0.1–0.5 mL/min). Under such flow rate conditions no real Langmuir adsorption isotherm was observed for CV, indicating that the adsorption equilibrium could not be reached. Nevertheless, even at pH 4.3, where by far the largest fraction of the silanol groups is not dissociated (a silica surface typically consists of 19% geminal or Q2 ($\text{pK}_a = 4.5$) and 81% vicinal or Q3 ($\text{pK}_a = 8.5$) silanol sites),¹⁵ adsorption of CV can still be observed, indicating that in addition to ionic interactions (induced) dipole interactions also play a role. For a detailed understanding about the adsorption mechanism, the possible existence of shearing effects and formation of a boundary layer should also be considered, but this is not within the scope of the current study. For DR10, adsorption effects appear to be far less important. The baseline of the absorption curve remained stable over a prolonged time and after repetitive injections of adsorbing dye; the prism surface did not degrade and could be used for days without cleaning. The baseline drift is acceptable (stable baselines for 45 minute measurements have been observed) and the tailing of the CV and DR10 peaks is comparable with the tailing observed in LC studies at a flow rate of 0.5 mL/min. This demonstrates that the surface of the prisms does not become contaminated and irreversibility of adsorption does not play a major role; the surface can be used for measurements over a prolonged timescale.

Typical flow-injection profiles of low CV concentrations (5–20 μM) at 0.5 mL/min can be seen in Fig. 2. Spikes on the baseline are sometimes observed due to the presence of air bubbles in the flow cell, despite the fact that all eluents were sonicated before use. At this flow rate the response of the system to CV does not change significantly with pH over the range of 4.3 to 8.8 (data not shown). The absolute absorbances observed in our flow system at 0.5 mL/min (linear flow 5.3 mm/s) are more than an order of magnitude lower than those

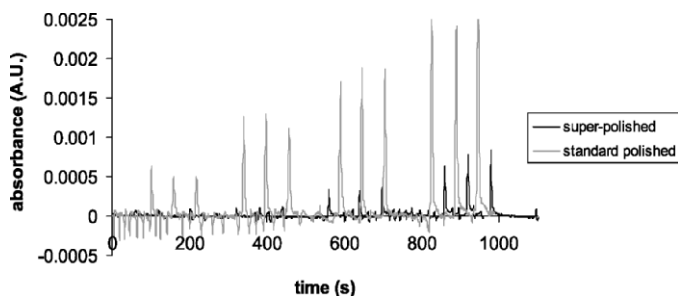


FIG. 2. Influence of surface roughness. FIA profiles showing triplicate injections of, respectively, 5, 10, 15, and 20 μM CV in 10 mM potassium phosphate buffer, pH = 7.4, on the super-polished and the standard polished TIR surface. The flow rate was 0.5 mL/min. The values on the y-axis are in absorbance units.

observed by Fisk et al.¹⁵ under semi-stationary conditions in a purely aqueous buffer. While Fisk et al. have successfully explained their observations with a multi-layer adsorption model, our system is far removed from equilibrium, thus complicating a detailed understanding of the data. On the standard polished surface, the response of CV is much stronger than on the super-polished surface, which is also obvious from the detection limits being 3 μM for the standard polished TIR surface and 5 μM for the super-polished TIR surface. These results indicate that for analytical purposes standard polished surfaces seem to be more appropriate. For the repeated injections the peak height variation is acceptable: typically 15%. Memory effects were not observed.

In Fig. 3, flow injection peak areas for CV are plotted as a function of concentration at 0.5 mL/min. Unexpectedly, the super-polished TIR surface gives a nonlinear response to CV, whereas for the standard polished surface a linear regression line is obtained. Overall, at lower concentrations the performance of the standard polished TIR surface is better, while at higher concentrations the responses on the two different surfaces are more similar. Upon reducing the flow rates to 0.3 or 0.1 mL/min, a similar nonlinear response to the CV concentration is observed for the standard polished surface (data not shown). We assume that the higher surface area of the standard polished surface is advantageous in the detection of low concentrations of CV. Additionally, the surface roughness of the standard polished prism might cause a turbulent flow at high flow rates, ensuring a more efficient exchange between the boundary layer and the bulk solution and thus stimulating further binding of CV. The flow regime inside the flow cell (laminar or turbulent) may be estimated from the Reynolds number:¹⁵

$$\text{Re} = \frac{\rho u d}{\mu} \quad (2)$$

where ρ is the density of the fluid (the density of water, 998 kg m^{-3} is assumed), μ is the dynamic fluid viscosity (0.8909×10^{-3} N s m^{-2}), and d is the thickness of the flow cell (10^{-3} m). u is the flow velocity; with the flow cell volume of 14 μL and length of 9 mm, this is 5.3, 3.2, or 1.1 mm s^{-1} for 0.5, 0.3, and 0.1 mL/min, respectively. Calculated Reynolds numbers are 5.9, 3.6, and 1.2, and the flow is likely to be turbulent (the critical Reynolds number is around 1; flows above this number are turbulent). Especially at low flows the flow regime will become more laminar, and as mentioned before, a nonlinear concentration dependence can be seen on the standard polished

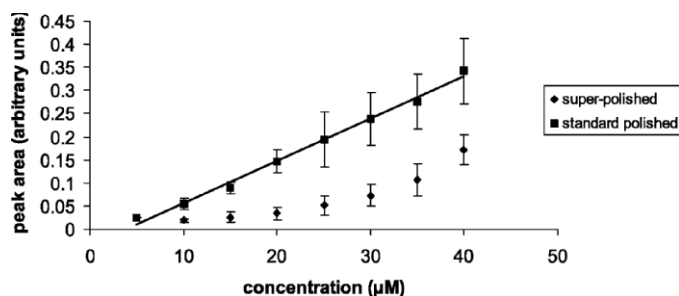


FIG. 3. Response curves of CV at a flow rate of 0.5 mL/min and a pH of 7.4 as observed on the standard polished and the super-polished TIR surface. Each concentration was measured in triplicate; the error bars represent one standard deviation.

surface upon lowering the flow rate as well. It seems therefore possible that the flow is in a transition from turbulent to laminar at the utilized flow rates and is more turbulent on the standard polished surface.

Contrary to CV, the DR10 response is linear for both the super-polished and standard polished TIR surface, also at low flow rates (see further below).

At low flow rates (0.1 mL/min) the tailing increased considerably (see Fig. 4), but within a time-span of minutes the ring-down time increased to the original value again. The width of the CV peak corresponds roughly to $1/\text{flowrate}$, whereas the area of the peak corresponds to $(1/\text{flowrate})^2$. At a flow rate of 0.5 mL/min and a pH of 4.3 (where most silanol groups will be neutral) the tailing was far worse than at pH 7.4 and 8.8 (data not shown), indicating that the adsorption of CV to silica is of a more irreversible nature.

For bulk absorbance, one can calculate the optical path length from the effective depth d_e for p -polarized (in the plane of the beam and the surface normal) light:²⁴

$$d_e = \frac{n_{21}\lambda(2\sin^2\theta - n_{21}^2)\cos\theta}{n_1\pi(1 - n_{21}^2)[(1 + n_{21}^2)\sin^2\theta - n_{21}^2](\sin^2\theta - n_{21}^2)^{1/2}} \quad (3)$$

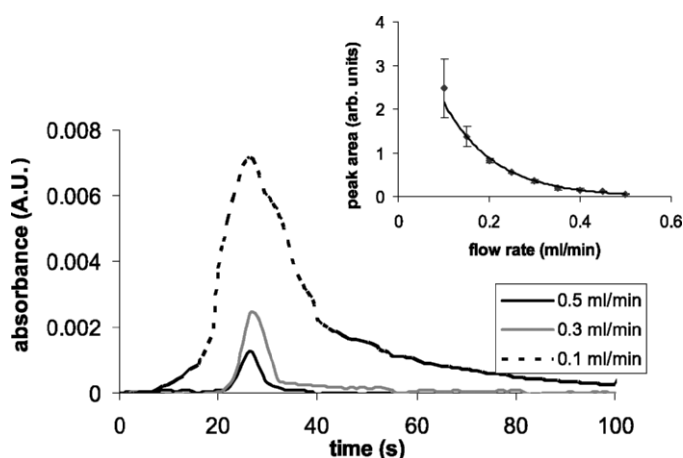


FIG. 4. Influence of flow rate on CV adsorption. Flow profiles showing an injection of 20 μM CV in 10 mM potassium phosphate buffer, pH = 7.4 on the super-polished TIR surface. Flow rates are 0.1, 0.3, and 0.5 mL/min; sample injection volume is 100 μL . Profiles were horizontally shifted for ease of comparison. The values on the y-axis are in absorbance units. The inset shows the peak area as a function of flow rate as measured for 20 μM CV on the standard polished TIR surface.

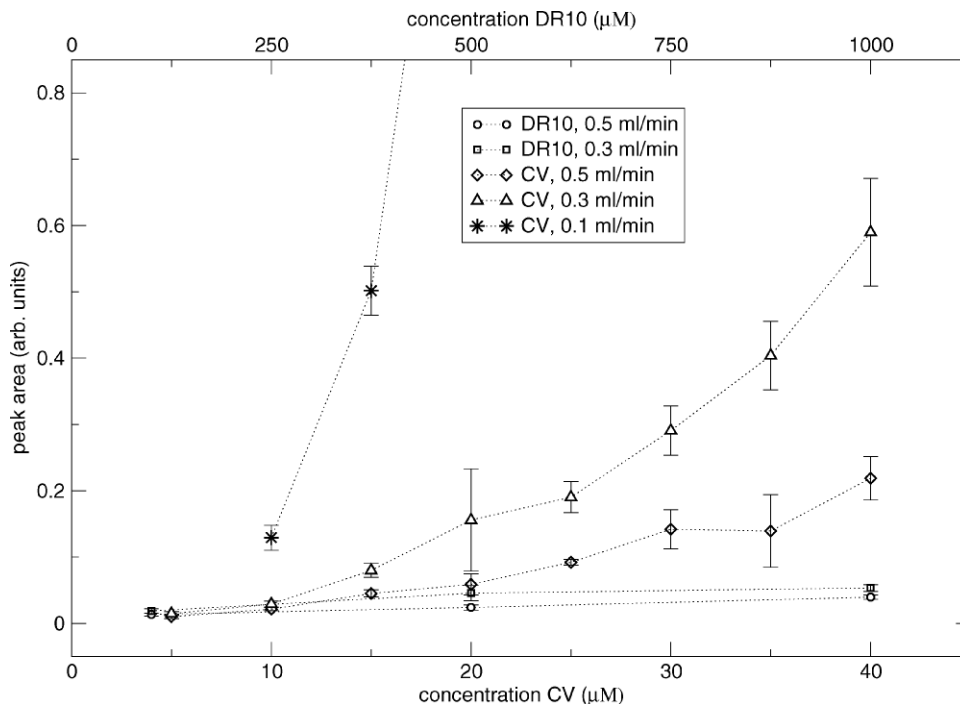


FIG. 5. Response curves of CV and DR10 at different flow rates and pH = 7.4 as observed on the super-polished TIR surface. Each concentration was measured in triplicate; the error bars represent one standard deviation. Injected concentrations of CV were varied between 5 and 40 μM (lower scale); those of DR10 ranged from 100 to 1000 μM (upper scale), plotted in the same graph for ease of comparison. Lines between the points are guides for the eye. For a flow of 0.1 mL/min only 2 data points are shown for CV since data points corresponding to higher concentrations are far off the shown vertical scale; for example, 40 μM of CV gave an area of 5.1.

where θ is the angle of incidence (72.8° in our case), λ is the wavelength of the light (532 nm), and n_1 and n_2 are the refractive indices of BK7 (1.52) and the liquid medium (1.33), respectively, and $n_{21} = n_2/n_1$. In the literature on infrared spectroscopy this effective path length is commonly used to compare absorbances in transmission mode with those obtained with an attenuated total reflection (ATR) geometry. For our setup we calculated a d_e of 403 ± 10 nm. The contribution of the bulk absorbance at a CV concentration of 20 μM using this d_e value is calculated as 4.2×10^{-5} A.U., assuming that the extinction coefficient of adsorbed CV equals that in bulk solution. This is much lower than the measured values: at a flow rate of 0.5 mL/min, the measured absorbance for the standard polished TIR surface is about 2.5×10^{-3} A.U. while it is 8×10^{-4} A.U. for the super-polished TIR surface (see Fig. 2). In fact, the observed absorption in EW-CRDS on the standard polished surface is about 60 times larger than expected based on the CV bulk concentration, indicating a significant enrichment at the surface. For DR10 the bulk absorbance at the detection limit of 100 μM is calculated to be 4×10^{-5} A.U. assuming that the extinction coefficients of adsorbed and bulk species are the same. The measured absorbance is on the order of 2×10^{-4} A.U. (data not shown), indicating that the hydrophilic dye DR10 also exhibits adsorption, but to a far lesser extent than CV.

To estimate the surface coverage in the case of CV, the relatively large footprint of the laser at the TIR surface (about 7 mm^2) should be considered. Assuming a probed layer thickness of roughly 400 nm, the detected volume is about 3 nL and the absolute detection limit is 9 fmol at the concentration limit of detection of 3 μM . Taking into account the enrichment factor of 60, the probed layer actually contains about 0.5 pmol of CV

on the probed surface area. Estimates for the number of available silanol sites range from 0.8 to 8 per square nm,¹⁵ which would correspond to 10 to 100 pmol on the probed surface (for the super-polished TIR surface). At this CV concentration, the actual surface coverage will therefore be on the order of 10^{-2} relative to the number of silanol groups.

Both CV and DR10 are hydrophilic dyes; the former is positively charged above pH 3, whereas the latter is negatively charged above pH 4. At a flow rate of 0.5 mL/min, CV has a response that is about 10 to 15 times higher than that of DR10, indicating that the EW-CRDS detection system has sufficient specificity to discriminate between species with different surface affinities. Whereas the response of the system towards DR10 at a pH of 7.4 is only increased in width upon lowering the flow rate from 0.5 to 0.3 mL/min, the peak area of 20 μM CV is three times higher at 0.3 mL/min. The CV response (peak area) increases roughly quadratically with decreasing flow rates (see Fig. 4, inset). A higher surface specificity is obtained if CV is given enough time to become adsorbed to the surface (see Fig. 5). Whereas for CV the performance of the standard polished TIR surface is better than that of the super-polished surface, the responses of both surfaces to DR10 are comparable.

Crystal Violet adsorption isotherms to silica with EW-CRDS have been measured by Shaw et al.;^{14,15} they used a syringe pump that delivered a very low flow of 4 mL/hour to a flow cell of 190 μL . Rather than using flow injection, they used a constant flow of CV solution at varying concentrations. They used purely aqueous buffer solutions without any modifier, causing the CV molecules to bind even more strongly to the surface, thus necessitating heavy cleaning after each measurement. Using a similar setup, their concentration detection limit

TABLE I. Peak area of 20 μM CV in eluents containing different buffers. Samples were dissolved in the same eluent as used.

Buffer	Area (arb. units)	Standard deviation ($n = 6$)
10 mM phosphate	0.061	0.0035
10 mM phosphate	0.025	0.0054
10 mM HEPES	0.080	0.0071
100 mM HEPES	0.037	0.0081

was about 0.3 μM of CV for a steady-state measurement, one order of magnitude lower than in our case. This difference should be attributed to a higher degree of surface binding achieved after complete equilibration, which will additionally be higher in water than in 50/50 water/methanol.

In order to study the influence of buffer ions (type and concentration), additional experiments have been carried out using 50% of 10 mM HEPES buffer at pH 7.4 in methanol. As expected, the flow-injection profiles for 20 μM CV were similar in shape, and somewhat higher absorbances were obtained than in phosphate buffer. HEPES and phosphate buffers were also tested at a higher concentration: 100 mM in methanol (50%, v/v). The results are summarized in Table I. The data were handled in the same way as for Figs. 3 and 5. It can be seen from the table that an increase in ionic strength leads to a decrease in CV adsorption. Furthermore, the signals as obtained for HEPES buffer are overall higher: this can be explained in a similar way. The ionic strength of a phosphate buffer containing a 10 mM mixture of HPO_4^{2-} and H_2PO_4^- will be higher than that of a 10 mM mixture of $\text{C}_8\text{H}_{17}\text{N}_2\text{SO}_4\text{H}$ and $\text{C}_8\text{H}_{17}\text{N}_2\text{SO}_4^-$.

CONCLUSION

In this study it has been demonstrated that EW-CRDS detection utilizing an anti-reflection coated Dove prism inside a linear cavity has distinct potential as a surface-selective detector in flow-injection and LC analysis. Only the analyte molecules present in a roughly 400 nm thick layer at the surface are detected, while the detection limits are, nevertheless, very low: 3 μM for Crystal Violet at a flow rate of 0.5 mL/min. Contamination or degradation of the surface is minimal, so that repeated measurements can be done over a prolonged time (days) without cleaning or re-alignment. At the applied flow rates the system is far from thermodynamic equilibrium. Nevertheless, the discrimination between the strongly adsorbing CV and the weakly adsorbing DR10 is quite efficient: already at 0.5 mL/min the response of the system towards CV is ten times higher. This discriminating power between non-adsorbing and adsorbing molecules increases significantly upon lowering the flow rates. The EW-CRDS response for CV was 60 times higher than expected if only bulk solution absorbance were to play a role in the absence of any binding to the surface. For DR10 the enrichment factor as a result of binding was much smaller, i.e., five times.

It should be noted that the ring-down times in this study were on the order of 5% of that of the empty cavity, mostly due to reflection losses. Therefore, substantial sensitivity improvement should be feasible. Using Brewster's angles for the entrance and exit faces of a Dove prism would lead to a decrease of only 40% of the ring-down time.¹⁹ However, such prisms are not easy to produce.

The current setup is capable of reproducible surface-specific adsorption and desorption of the compound of interest at flow rates that are compatible with FIA and LC studies. Future applications of the EW-CRDS setup include specific LC detection or biosensing. Since coating of silanol with, for instance, single-stranded DNA or antibodies is well studied and widespread in bioanalytical chemistry and biological techniques and coating runs are even commercially available, modification of the silica TIR face of the prism surface and surface-specific detection should be feasible.

1. K. L. Bechtel, R. N. Zare, A. A. Kachanov, S. S. Sanders, and B. A. Paldus, *Anal. Chem.* **77**, 1177 (2005).
2. L. van der Sneppen, A. E. Wiskerke, F. Ariese, C. Gooijer, and W. Ubachs, *Appl. Spectrosc.* **60**, 935 (2006).
3. P. Claudon, M. Donner, and J. F. Stoltz, *J. Mater. Sci. Mater. Med.* **2**, 197 (1991).
4. T. Vo-Dinh, M. J. Sepianak, G. D. Griffin, and J. P. Alarie, *Immunomethods* **3**, 85 (1993).
5. S. Rodriguez-Mozaz, M.-P. Marco, M. J. Lopez de Alda, and D. Barcelo, *Anal. Bioanal. Chem.* **378**, 588 (2004).
6. A. C. R. Pipino, J. W. Hudgens, and R. E. Huie, *Rev. Sci. Instrum.* **68**, 2978 (1997).
7. A. C. R. Pipino, J. W. Hudgens, and R. E. Huie, *Chem. Phys. Lett.* **280**, 104 (1997).
8. A. C. R. Pipino, *Phys. Rev. Lett.* **83**, 3093 (1999).
9. A. C. R. Pipino, J. P. M. Hoefnagels, and N. Watanabe, *J. Chem. Phys.* **120**, 2879 (2004).
10. I. M. P. Aarts, A. C. R. Pipino, J. P. M. Hoefnagels, W. M. M. Kessels, and M. C. M. Van de Sanden, *Phys. Rev. Lett.* **95**, 166104 (2005).
11. M. Gupta, H. Jiao, and A. O'Keefe, *Opt. Lett.* **27**, 1878 (2002).
12. R. Brown, I. Kozin, Z. Tong, R. Oleschuk, and H.-P. Looock, *J. Chem. Phys.* **117**, 10444 (2002).
13. P. B. Tarsa, P. Rabinowitz, and K. K. Lehmann, *Chem. Phys. Lett.* **383**, 297 (2004).
14. A. M. Shaw, T. E. Hannon, F. Li, and R. N. Zare, *J. Phys. Chem. B* **107**, 7070 (2003).
15. J. D. Fisk, R. Batten, G. Jones, J. P. O'Reilly, and A. M. Shaw, *J. Phys. Chem. B* **109**, 14475 (2005).
16. W. B. Martin, S. Mirov, D. Martyshkin, and R. Venugopalan, *J. Biomed. Opt.* **10**, 024025 (2005).
17. F. Li and R. N. Zare, *J. Phys. Chem. B* **109**, 3330 (2005).
18. T. E. Hannon, S. Chah, and R. N. Zare, *J. Phys. Chem. B* **109**, 7435 (2005).
19. H.-F. Fan, C.-Y. Hung, and K.-C. Lin, *Anal. Chem.* **78**, 3583 (2006).
20. M. Mazurenka, L. Wilkins, J. V. Macpherson, P. R. Unwin, and S. R. Mackenzie, *Anal. Chem.* **78**, 6833 (2006).
21. M. A. Everest, V. M. Black, A. S. Haehlen, G. A. Haveman, C. J. Kliewer, and H. A. Neill, *J. Phys. Chem. B* **110**, 19461 (2006).
22. S. E. Fiedler, A. Hese, and A. A. Ruth, *Chem. Phys. Lett.* **371**, 284 (2003).
23. H. Naus, I. H. M. van Stokkum, W. Hogervorst, and W. Ubachs, *Appl. Opt.* **40**, 4416 (2001).
24. N. J. Harrick, *Infrared Reflection Spectroscopy* (Harrick Scientific Corporation, New York, 1987).